ELSEVIER

Composites Science and Technology 62 (2002) 2189–2199

COMPOSITES SCIENCE AND TECHNOLOGY

www.elsevier.com/locate/compscitech

A low cycle fatigue model of a short-fibre reinforced 6061 aluminium alloy metal matrix composite

H.-Z. Ding[1], H. Biermann[2]*, O. Hartmann

Universität Erlangen-Nürnberg, Institut für Werkstoffwissenschaften, Lehrstuhl I, Martensstr. 5, 91058 Erlangen, Germany

Received 11 March 2002; received in revised form 26 July 2002; accepted 29 July 2002

Abstract

A low cycle fatigue model has been developed to predict the fatigue life of both the unreinforced aluminium alloy and the short-fibre reinforced aluminium alloy metal-matrix composites based solely on crack propagation from microstructural features. In this approach a crack is assumed to initiate and grow from a microstructural feature on the first cycle. The model assumes that there is a fatigue-damaged zone ahead of the crack tip within which the actual degradation of the material takes place. The low-cycle fatigue crack growth and the condition for failure are controlled by the amount of cyclic plasticity generated within the fatigue-damaged zone ahead of the crack tip and by the ability of the short fibres to constrain this cyclic plasticity. The fatigue crack growth rate is directly correlated to the range of crack-tip opening displacement. The empirical Coffin–Manson and Basquin laws have been derived theoretically and applied to compare with total-strain controlled low-cycle fatigue life data obtained on the unreinforced 6061 aluminium alloy at 25 °C and on the aluminium alloy AA6061 matrix reinforced with Al_2O_3 Saffil short-fibres of a volume fraction of 20 vol.% and test temperatures from −100 to 150 °C. The proposed model can give predicted fatigue lives in good agreement with the experimental total-strain controlled fatigue data at both high strain low-cycle fatigue and low strain high-cycle fatigue regime. It is remarkable that the addition of high-strength Al_2O_3 fibres in the 6061 aluminium alloy matrix will not only strengthen the microstructure of the 6061 aluminium alloy, but also channel deformation at the tip of a crack into the matrix regions between the fibres and therefore constrain the plastic deformation in the matrix. The overall expected effect is therefore the reduction of the fatigue ductility.

Keywords: A. Metal-matrix composites (MMCs); B. Fatigue; B. Modelling; C. Crack; D. Life prediction

1. Introduction

Short-fibre reinforced metal-matrix composites (MMCs), in particular those based on a commercially used aluminium alloy, are being used e.g. in the automotive industry. This is because the short-fibre reinforced MMCs exhibit attractive advantages, such as improved stiffness, higher strength and superior wear resistance and in particular elevated-temperature properties compared with the constituent matrix materials [1–3]. However, the short-fibre reinforcement also leads to poor ductility and low fracture toughness [4–6]. To be able to use fully the properties of this kind of materials, a knowledge of fatigue behaviour and an improved understanding of strain-controlled low-cycle fatigue (LCF) damage tolerance characteristics in these materials is outstandingly required [7,8].

The strain-controlled LCF behaviour of short-fibre reinforced MMCs has received much less attention than that of particulate- and/or continuous fibre-reinforced MMCs, both in *theory* and *experiment*. The present state of understanding of LCF behaviour in short-fibre reinforced MMCs is still in its infancy. Elementary methods of solid mechanics are easily applied to continuous fibre–matrix composite systems to predict the strength and life behaviours. In short-fibre reinforced MMCs, however, the analysis becomes complicated due

* Corresponding author. Tel.: +49-3731-393564; fax: +49-3731-393703.

E-mail addresses: hong-zhi.ding@man.ac.uk (H.-Z. Ding), biermann@ww.tu-freiberg.de (H. Biermann).

[1] Current address: University of Manchester, School of Engineering, Oxford Road, Manchester M13 9PL, UK.

[2] Current address: Technische Universität Bergakademie Freiberg, Institut für Werkstofftechnik, Gustav-Zeuner-Str. 5, 09599 Freiberg, Germany.

0266-3538/02/$ - see front matter
PII: S0266-3538(02)00160-4

to the discontinuities at the fibre ends and it has been experimentally found that high stress concentrations occur at the fibre ends. The discontinuities at the fibre ends result in very complicated fatigue damage and failure mechanisms and therefore create greater difficulties in fatigue life calculations. In the literature, only limited data on the LCF behavior of short-fibre reinforced MMCs are available so far. Williams and Fine [9] studied the cyclic deformation properties of SiC-whisker-reinforced 2124 aluminium alloys and found that the cyclic yield strength of the composite is significantly higher than that of the unreinforced alloy at the same aging condition. Hurd [10] studied Saffil short-fibre reinforced Al–Mg–Si and Al–Si composites in strain-controlled LCF. He found that in the Al–Si alloys, which are weakened by the addition of the short Saffil fibres, the LCF properties of the composite were inferior to the unreinforced alloy; however, in the Al–Mg–Si alloys, which are strengthened by fibre addition, the LCF properties were comparable. Harris [11] showed that in the case of cast Al–Cu–Mg composites reinforced with Saffil short fibres, where the yield strength of the composites exceeded that of the unreinforced alloy, their fatigue strengths for both high-cycle fatigue (HCF) and LCF were superior. Levin and Karlsson [12] tested strain-controlled LCF properties of 6061 aluminium alloy, 15 vol.% SiC particulate and 20 vol.% Saffil short fibre reinforced 6061 aluminium alloy, respectively. Through a systematic study of surface crack initiation and growth during LCF, they demonstrated that crack initiation from broken large fibres or particles is instantaneous (Saffil composite) or almost instantaneous (SiCp composite). They further observed that the growth properties of individual microcracks determine the LCF life in the composites irrespective of the cyclic strain amplitude. Their results also show that the LCF properties of the Saffil short-fibre reinforced aluminium alloy MMC were inferior to the unreinforced alloy. Hartmann et al. [13] studied the cyclic deformation behaviour of three MMCs, i.e. AA6061-T6 reinforced with 20 vol.% alumina particles and short-fibres, respectively, and pure aluminium reinforced with 20 vol.% alumina short-fibres at temperatures between $T=-100$ °C and $T=300$ °C in total-strain controlled symmetrical push–pull fatigue tests. They showed that short-fibre reinforced composites, both with alloyed and unalloyed aluminium matrix, harden cyclically more than the particulate-reinforced composite [13–15].

The objective of this article is to present a quantitative description of the fatigue damage evolution process in both unreinforced aluminium alloy and short-fibre reinforced aluminium alloy metal-matrix composites, and derive a fatigue life prediction model based on specific microstructural mechanisms. This is achieved by applying the authors' very recent model for the LCF life of particulate reinforced MMCs [16] as well as short-fibre reinforced pure aluminium MMCs [17]. The first stage of this study has been experimental. The results are used as input and validation data for the model. The LCF damage mechanisms identified at the reinforcement scale, by means of a fatigue damaged zone, are included in our model. The LCF crack growth and life are then predicted from material properties, loading conditions and micro-mechanisms. The validity of the theoretical model is evaluated with experimental data of the unreinforced 6061 aluminium alloy and a 20 vol.% Al_2O_3 short-fibre reinforced 6061 aluminium-matrix composite.

2. Experimental work

The materials tested in this study are the unreinforced 6061 aluminium alloy (AA6061) and the 6061 aluminium alloy reinforced with a volume fraction of 20 vol.% Al_2O_3 short fibres (AA6061-Al_2O_3-20s). The microstructure of such short-fibre reinforced MMCs, as shown in Fig. 1, has been characterised in detail earlier [15]. The Saffil fibres have a diameter of approximately $d=3$ μm and a mean length of about $l=200$ μm. The fibres are arranged in a planar and random manner in the gas-pressure infiltrated short-fibre reinforced composite. Therefore, the MMCs are composed of a ductile matrix and randomly-planar oriented brittle fibres. Due to the production process, a fibre content of 20 vol.% is achieved in the pre-forms which can be obtained commercially.

The fatigue test specimens used in this study were smooth cylindrical bars with a diameter of 5 mm in the gage section. The samples of both AA6061 and AA6061-Al_2O_3-20s were aged to peak hardness T6 (the specimens were solution treated at 560 °C for 0.5 h, followed by water quenching; the composite specimens were then hardened at 165 °C for 8 h; the AA6061 specimens were swaged after solution heat treatment, hardened at 400 °C for 10 min and finally water cooled to obtain a fine grain size comparable to the matrix of

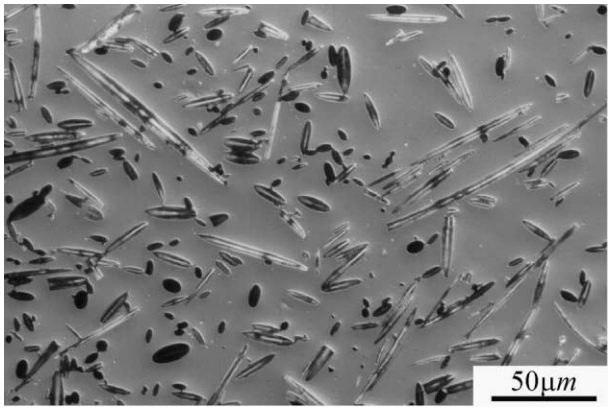

Fig. 1. Optical micrograph of 20 vol.% short-fibre reinforced AA6061-T6 in the undeformed condition.

the composite, respectively), controlled by hardness tests (see [15]). After mechanical grinding and polishing, isothermal, total-strain controlled fatigue tests were carried out with total-strain amplitudes ranging between $\Delta\varepsilon_t/2 = 0.001$ and $\Delta\varepsilon_t/2 = 0.01$ (strain ratio $R_{\varepsilon_t} = -1$, total-strain rate $\dot{\varepsilon}_t = 0.002/s$) in servo-hydraulic universal testing machines. Strain was measured with a clip-on extensometer attached directly to the gauge length at low and at room temperature and with a high-temperature extensometer equipped with alumina rods at elevated temperature. The fatigue failure criterion was defined as drop in maximum tensile load of about 20% or specimen fracture, respectively. The LCF behaviour of AA6061-T6 was investigated experimentally only at room temperature (25°C), but AA6061-Al_2O_3-20s-T6 was tested in the temperature range between $T = -100$ °C and $T = 150$ °C in total-strain controlled symmetrical push–pull fatigue tests [13–15].

The cyclic stress–strain (CSS) curves, as shown in Fig. 2, were obtained from a series of strain-controlled tests at different total-strain amplitudes. These curves describe the relationship between cyclic flow stress and cyclic plastic strain amplitude, and can be expressed by a power function i.e.

$$\frac{\Delta\sigma}{2} = K'\left(\frac{\Delta\varepsilon_{\mathrm{pl}}}{2}\right)^{n'} \tag{1}$$

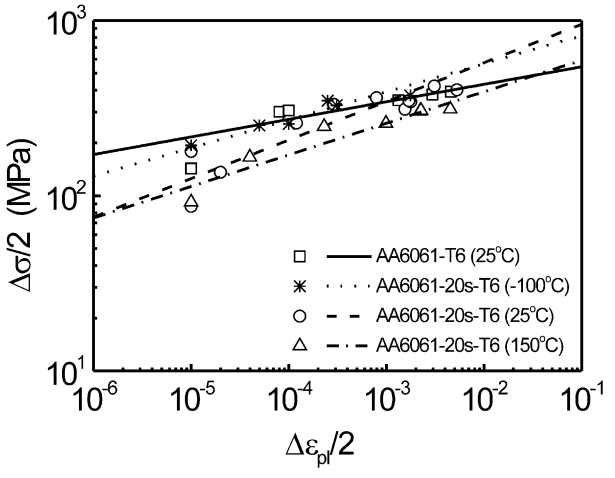

Fig. 2. Cyclic stress–strain curves of AA6061-T6 and AA6061-20s-T6.

where $\Delta\sigma/2$ is the steady-state stress amplitude, $\Delta\varepsilon_{\mathrm{pl}}/2$ is the cyclic plastic strain amplitude in the whole bulk of the material, n' the cyclic strain hardening exponent which provides a measurement of the materials response to cyclic strain and K' is the cyclic strain hardening coefficient. Since both materials show varying stress amplitudes with increasing number of cycles (for details of cyclic hardening and/or softening see [13–15]), no steady-state stress amplitude could be achieved. Therefore, $\Delta\sigma/2$ and $\Delta\varepsilon_{\mathrm{pl}}/2$ were both taken at half the fatigue life of the specimens in the present study. Values of n' and K' are given in Table 1. Here, the composite's cyclic yield strength $R_{\mathrm{p,c}}$ is regarded as the stress amplitude for the plastic strain amplitude $\Delta\varepsilon_{\mathrm{pl}}/2 = 0.2\%$, i.e. $R_{\mathrm{p0.2,c}} = K'(0.002)^{n'}$, determined from the CSS curves.

Experimental observations have shown that LCF crack initiation occurs always at or under the surface and the crack grows along regions containing locally high amounts of short fibres. Fig. 3 includes two scanning electron micrograph (SEM) images of a total strain-controlled LCF specimen deformed at room temperature and $\Delta\varepsilon_t/2 = 0.002$. Fig. 3a shows the crack path and Fig. 3b the crack tip and the damaged zone clearly visible ahead of the crack tip. The damage mode is found to be mainly fibre cracking or fibre–matrix interface debonding.

3. Model development

3.1. LCF model for unreinforced aluminium alloy

In this part we first present a LCF model for the unreinforced aluminium alloy. The analysis we developed involves modelling both the crack-tip cyclic plastic deformation characteristics and the crack-growth kinetic characteristics taking into account the conditions of large-scale yielding (LSY) in the case of high-strain LCF. In the following development we first describe the crack-tip cyclic plastic deformation processes. We then proceed to develop a microstructure-based LCF crack-growth rate formula. Finally, we calculate the LCF life and derive theoretically both Coffin–Manson and Basquin laws.

It is well established that in metals there is a cyclic plastic zone (CPZ) ahead of the crack tip under fatigue loading, and the CPZ includes a fatigue damaged zone

Table 1
Cyclic stress–strain data and mechanical parameters of AA6061-T6 and AA6061-Al_2O_3-20s-T6

Material	T (°C)	E_{m} (GPa)	E_{f} (GPa)	E_{c} (GPa)	n'	K' (MPa)	$R_{\mathrm{p,C}}$ (MPa)
AA6061-T6	25	71	–	–	0.10	685	368
AA6061-20s-T6	−100	72.5	300	91	0.16	1183	438
	25	71	300	89	0.22	1579	402
	150	67	300	87	0.18	898	293

(FDZ) very close to the crack tip within which the local severe shearing process takes place during crack growth [18–20]. The stress level in the FDZ is limited to the fracture stress or the ultimate tensile strength (UTS) of the materials. A variety of theories have been developed to predict the sizes of CPZs. These theories were first employed as correction factors for fracture mechanics calculations. Under small scale yielding (SSY) condition, the linear elastic fracture mechanics (LEFM) has been used to provide a description of fatigue crack propagation which is related to ΔK at the crack tip. The CPZ size, r_{cp}, may be estimated generally as [21]

$$r_{cp} = \lambda\left(\frac{\Delta K}{2R_p}\right)^2 \tag{2}$$

Here $\Delta K = (\Delta\sigma)Y\sqrt{\pi a}$ is the applied stress intensity range, a is the crack length, Y is a crack geometry correction factor, $2R_p$ is the cyclic yield stress, λ is a CPZ correction factor that denotes the best-fit proportionality factor between r_{cp} and $\left(\Delta K/2R_p\right)^2$. The stress and strain distribution within the CPZ, as has been proposed by Rice [21], can be described as

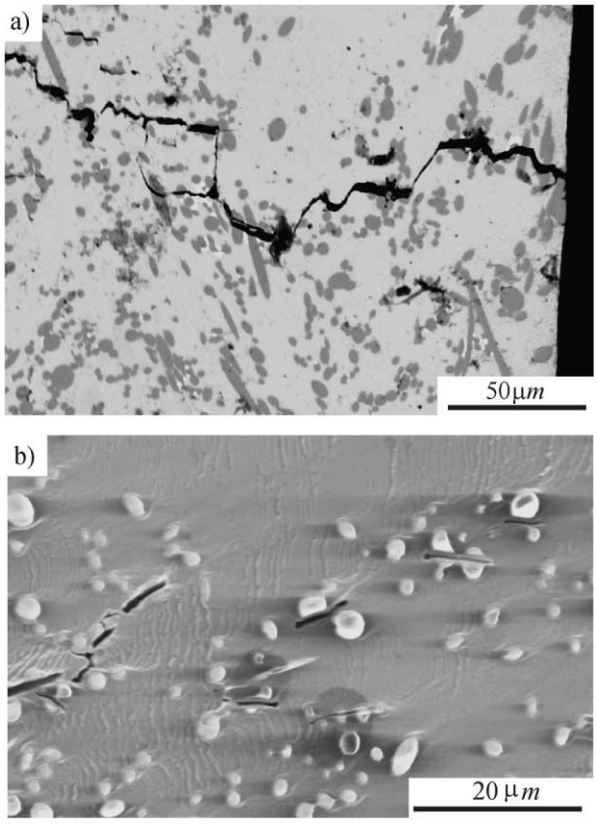

Fig. 3. SEM image of 20 vol.% short-fibre reinforced AA6061 after cyclic deformation ($\Delta\varepsilon_t/2 = 0.002$, $T = 25\ ^\circ C$): (a) crack growth path; (b) crack-tip fatigue-damaged zone (the section was prepared by ion etching).

$$\frac{\Delta\sigma(r)}{2} \propto (r\ (\mathrm{cp})/r)(n'/(n'+1)) \tag{3}$$

$$\frac{\Delta\varepsilon_{pl}(r)}{2} \propto (r\ (\mathrm{cp})/r)(1/(n'+1)) \tag{4}$$

When the SSY condition is violated or extended plastic deformation occurs ahead of the crack tip, which is just our concern in the case of high-strain LCF, a satisfactorily accurate estimate of the cyclic plastic deformation range or r_{cp} cannot be provided by the aforementioned LEFM approach. The necessary of including the influence of significant crack tip cyclic plastic deformation on the prediction of the local carrying capacity of a flawed material has been the major impetus for the development of elastic–plastic fracture mechanics (EPFM) during the last four decades. It has been suggested that the cyclic plastic deformation is always accumulated ahead of the crack tip with the advance of cycle number from the time, irrespective of the yielding condition. Without loss of generality, it is reasonable to hypothesise that the CPZ still exists and the CPZ size still depends upon the value of $\left(\Delta K/2R_p\right)^2$ even in the general yielding condition. Therefore, under the high-strain LCF condition, the CPZ size can be approximately calculated as

$$\begin{aligned} r_{cp} &= \lambda\left(\frac{\Delta K}{2R_p}\right)^2 \equiv \lambda\pi Y^2\left(\frac{\Delta\sigma}{2R_p}\right)^2 a \\ &= \lambda\pi Y^2\left(\frac{K'}{R_p}\right)^2\left(\frac{\Delta\varepsilon_{pl}}{2}\right)^{2n'} a \end{aligned} \tag{5}$$

A more specific verification on this assumption will be addressed again in Section 4.1. The corresponding stress and strain distribution within the CPZ can be determined in terms of Eqs. (3) and (4) as

$$\frac{\Delta\sigma(r)}{2} = (\Delta\sigma/2)(r\ (\mathrm{cp})/r)(n'/(n'+1)) \tag{6}$$

$$\frac{\Delta\varepsilon_{pl}(r)}{2} = (\Delta\varepsilon\ (\mathrm{pl})/2)(r\ (\mathrm{cp})/r)(1/(n'+1)) \tag{7}$$

From Eqs. (5) and (6) and using the condition that the local cyclic stress level approaches the ultimate tensile strength of the unreinforced aluminium alloy, R_m, we can calculate the size of the FDZ as

$$r_{FDZ} = \lambda\pi Y^2\left((K')^{3+1/n'}/R_m^{1+1/n'}\left(R_p\right)^2\right)\left(\frac{\Delta\varepsilon_{pl}}{2}\right)^{3n'+1} a \tag{8}$$

By using Eqs. (7) and (8), we can calculate the accumulated average plastic strain, ε^*_{pl}, in the FDZ as

$$\varepsilon^*_{\mathrm{pl}} = \frac{1}{r_{\mathrm{FDZ}}}\int_0^{r_{\mathrm{FDZ}}} \left(\Delta\varepsilon_{\mathrm{pl}}(r)/2\right)\mathrm{d}r = \frac{n'+1}{n'}\left(\frac{R_{\mathrm{m}}}{K'}\right)^{1/n'} \tag{9}$$

According to Rice [22], the J integral can be calculated in general as

$$J = -\frac{\partial V}{\partial a} \tag{10}$$

In view of the LCF crack growth being controlled by the FDZ around the crack tip, it may be suggested that the potential energy V in the J integral equation is approximately equal to the interaction energy V_{int} between the FDZ and the crack-tip stress–strain field. So, the local driving force acting on the FDZ around the crack tip is just the local driving force for fatigue crack growth in nature. The interaction energy V_{int} can be calculated as [23]

$$V_{\mathrm{int}} = -\int_v \sigma^*\varepsilon^*_{\mathrm{pl}}\mathrm{d}u \tag{11}$$

where σ^* is the local cyclic stress amplitude, $\varepsilon^*_{\mathrm{pl}}$ is the accumulated average plastic strain and the integral is taken over the FDZ volume. In determining the size of the crack-tip FDZ, we have assumed that within the FDZ the local cyclic stress is uniform and $\sigma^* = R_{\mathrm{m}}$. The accumulated average plastic strain $\varepsilon^*_{\mathrm{pl}}$ can be determined by Eq. (9). Therefore, for the interaction energy per unit size along the direction that is perpendicular to the crack plane, Eq. (11) reduces to

$$V_{\mathrm{int}} = -R_{\mathrm{m}}\varepsilon^*_{\mathrm{pl}}\pi(r_{\mathrm{FDZ}}/2)^2 \tag{12}$$

By substituting Eqs. (8), (9) and (12) into Eq. (10), we finally have

$$\Delta J = -\frac{\partial V_{\mathrm{int}}}{\partial r_{\mathrm{FDZ}}} = \frac{\lambda\pi^2 Y^2}{2}\left(\frac{n'+1}{n'}\right)\left(\frac{(K')^3}{(R_{\mathrm{p}})^2}\right)\left(\frac{\Delta\varepsilon_{\mathrm{pl}}}{2}\right)^{3n'+1} a \tag{13}$$

According to the result of fracture mechanics, the cyclic J integral is directly related to the range of crack-tip opening displacement ($\Delta CTOD$) and approximately, $\Delta CTOD = \Delta J/R_{\mathrm{p}}$. Naturally, we can calculate $\Delta CTOD$ as

$$\Delta CTOD = \frac{\lambda\pi^2 Y^2}{2}\left(\frac{n'+1}{n'}\right)\left(\frac{K'}{R_{\mathrm{p}}}\right)^3\left(\frac{\Delta\varepsilon_{\mathrm{pl}}}{2}\right)^{3n'+1} a \tag{14}$$

Following the example of Tomkins [19], the LCF crack growth rate could be calculated by assuming that the fatigue crack extension per cycle, δa, is directly proportional to the change in the crack-tip opening displacement, $\Delta CTOD$. This gives $\delta a \propto \Delta CTOD$. Replacing the proportionality sign with equality sign gives $\mathrm{d}a/\mathrm{d}N = \eta\Delta CTOD$, where η is a proportionality constant/factor. In the study, we use the value of $\eta = 1/2$, i.e. we assume that the fatigue crack extension per cycle is directly equal to one half of the range of the crack-tip opening displacement, in the manner of Tomkins. Therefore, we have

$$\frac{\mathrm{d}a}{\mathrm{d}N} = \frac{\lambda\pi^2 Y^2}{4}\left(\frac{n'+1}{n'}\right)\left(\frac{K'}{R_{\mathrm{p}}}\right)^3\left(\frac{\Delta\varepsilon_{\mathrm{pl}}}{2}\right)^{3n'+1} a \tag{15}$$

This is the LCF crack growth rate of the unreinforced aluminium alloy derived according to the present study. In view of the microstructure mechanism of LCF damage development as described above, the number of fatigue crack growth cycles to failure can be calculated by integrating Eq. (15) from an initial crack size a_{i} to a critical crack size a_{f}. The fatigue life formula in the form of the Coffin–Manson law [24,25] is obtained as follows

$$\frac{\Delta\varepsilon_{\mathrm{pl}}}{2} = \left\{\frac{8n'}{\lambda\pi^2 Y^2(n'+1)}\left(\frac{R_{\mathrm{p}}}{K'}\right)^3 \ln\left(\frac{a_{\mathrm{f}}}{a_{\mathrm{i}}}\right)\right\}^{\frac{1}{3n'+1}} (2N_{\mathrm{f}})^{-1/(3n'+1)} \tag{16}$$

By using the CSS Eq. (1) and the above equation, we can easily derive the following stress vs. life relationship in the form of a Basquin law [26]

$$\frac{\Delta\sigma}{2} = K'\left\{\frac{8n'}{\lambda\pi^2 Y^2(n'+1)}\left(\frac{R_{\mathrm{p}}}{K'}\right)^3 \ln\left(\frac{a_{\mathrm{f}}}{a_{\mathrm{i}}}\right)\right\}^{\frac{n'}{3n'+1}} (2N_{\mathrm{f}})^{-n'/(3n'+1)} \tag{17}$$

3.2. LCF model for short-fibre reinforced aluminium alloy MMCs

It is a very reasonable thing to extend the concepts of both CPZ and FDZ under the high-strain LCF condition from the unreinforced aluminium alloy into the short-fibre reinforced aluminium alloy MMC. However, the strong influence of the particular microstructure of the short-fibre reinforced MMC on the crack-tip cyclic plastic deformation will have to be taken into account. In our consideration, the actual degradation process of the composite material takes place within the crack-tip FDZ. Many factors may be involved in the actual degradation process, they include such as the brittle nature of fibres, plastic flow constraint of the metallic matrix due to the presence of reinforcement fibres, stress concentration, increased dislocation density near the interface and the hydrostatic stresses within the constrained matrix. Fatigue crack growth in the short-fibre reinforced MMCs is substantially controlled by the state of the localised plastic deformation in the FDZ very near the crack tip.

Following the example of above, we begin by assuming that the size of the CPZ of the short-fibre reinforced MMC should be calculated as

$$r_{cp} = \lambda\left(\frac{\Delta K_{eff}}{2R_{p,m}}\right)^2 = \lambda\pi Y^2\left(\frac{\Delta\sigma_{eff}}{2R_{p,m}}\right)^2 a \tag{18}$$

where λ is still a CPZ correction factor for the short-fibre reinforced MMCs, $\Delta K_{eff} \equiv (\Delta\sigma_{eff})Y\sqrt{\pi a}$ is now the effective stress intensity factor range, a and Y are the crack length and crack geometry correction factor, respectively, $\Delta\sigma_{eff}/2$ is the effective stress amplitude and $R_{p,m}$ is the matrix yield strength. Comparing with Eq. (5), the important modifications in Eq. (18) have been done, in view of the facts: (1) Only the matrix can deform plastically in short-fibre reinforced MMCs due to the brittle nature and high elastic modulus of the reinforcement fibres. This explains why we use $R_{p,m}$ but not $R_{p,c}$, the composite's cyclic yield strength. (2) Non-deforming reinforcement fibres channel deformation at the tip of a crack into the matrix regions between short fibres, and short fibres also constrain flow in the matrix and therefore reduce the deformation that can occur. This effect has been shown in particulate-reinforced MMCs [27–32] and explains why we use ΔK_{eff}, an effective stress intensity factor range [33,34]. The validity and feasibility of Eq. (18) has been proved very recently by the authors for LCF behaviour of particulate reinforced MMCs [16] and a short-fibre reinforced pure aluminium matrix MMC [17].

In order to connect the microstructure with the macroscopic properties of the composite, in the following, a modified rule of mixtures (MROM) approach that was proposed first by Friend [2] is employed to calculate the cyclic yield strength of randomly-planar oriented short-fibre reinforced aluminium MMCs:

$$R_{p,C} = C_1\left(\frac{E_f}{E_m}\right)\left(1 - \frac{dE_f}{2lE_m}\right)V_f R_{p,m} + C_2(1 - V_f)R_{p,m} \tag{19}$$

where $R_{p,C}$ represents the effective composite yield strength, $R_{p,m}$ is the reference matrix yield strength; d and l are the short-fibre diameter and length, respectively; V_f is the volume fraction of the fibres; E_m and E_f are the Young's moduli of the matrix and fibres, respectively. C_1 is the fibre orientation factor describing the discontinuous nature and random orientation of the fibres; C_2 is the matrix characteristic factor depending on the matrix employed and describing both the dislocation strengthening of the matrix by thermal residual stresses and the dispersion strengthening of the matrix due to the presence of the randomly-oriented short-fibre arrays. In the case of a randomly planar orientation of the fibres, the value of C_1 is 3/8; for the aluminium alloy AA6061, the value of C_2 is 1, as reported by Friend [2].

In order to assess the level of local constraint, Davidson and McClung [30] have proposed that the level of constraint in the crack-tip region can be computed from strain values measured in the vicinity of the crack tip, and constraint (C_ε) can be defined generally as the ratio of mean to effective strains (or stresses). With this definition they have also developed a technique for experimentally assessing the local level of constraint from the measured response of the material near a fatigue crack tip in alloys and particulate-reinforced MMCs. Following this general definition of the constraint and without loss of generality, we propose that the effective stress amplitude acting on the crack can be calculated as

$$\frac{\Delta\sigma_{eff}}{2} = \frac{1}{2C_\varepsilon}\left(\frac{\Delta\sigma}{2}\right) = \frac{K'}{2C_\varepsilon}\left(\frac{\Delta\varepsilon_{pl}}{2}\right)^{n'} \tag{20}$$

Here C_ε is the local constraint that is introduced by the short fibres. As defined [30], $0 \leqslant C_\varepsilon \leqslant 0.5$, where a higher value denotes higher constraint. To be specific, the higher is the local constraint, the lower the deformation that can occur in the regions between the short fibres, and therefore the lower the effective stress. For the maximum constraint, $C_\varepsilon = 0.5$, we have $\Delta\sigma_{eff}/2 = \Delta\sigma/2$, this means that all deformation at the crack tip is completely constrained, and is, therefore, approximately elastic [35]. For a particulate-reinforced aluminium alloy composite, constraint in the matrix between particles is found to be of the order of 0.1–0.3 [30]. Approximately, if we take $C_\varepsilon = 0.20$ as the average value of the constraint in the aluminium alloy matrix between short fibres, we can then obtain $\Delta\sigma_{eff}/2 = 2.5(\Delta\sigma/2)$, this result is well consistent with the results of FE modelling of deformation in short-fibre reinforced MMCs, e.g. Ref. [12]. This value of the constraint will be used later to predict fatigue lives.

Substituting Eqs. (19) and (20) into Eq. (18), we finally get after calculation

$$r_{cp} = \frac{\lambda\pi Y^2}{4C_\varepsilon^2}\left[\frac{C_1E_fV_f}{E_m}\left(1 - \frac{dE_f}{2lE_m}\right) + C_2(1 - V_f)\right]^2\left(\frac{K'}{R_{p,c}}\right)^2\left(\frac{\Delta\varepsilon_{pl}}{2}\right)^{2n'}a \tag{21}$$

In the exact same manner used in the case of the unreinforced aluminium alloy, we can finally have the ΔJ of short-fibre reinforced MMCs as

$$\Delta J = \frac{\lambda\pi^2 Y^2}{8C_\varepsilon^2} \times \left[\frac{C_1E_fV_f}{E_m}\left(1 - \frac{dE_f}{2lE_m}\right) + C_2(1 - V_f)\right]^2\left(\frac{n'+1}{n'}\right) \times \left(\frac{(K')^3}{(R_{p,c})^2}\right)\left(\frac{\Delta\varepsilon_{pl}}{2}\right)^{3n'+1}a. \tag{22}$$

The LCF crack growth rate, da/dN, is directly related to the local driving force acting upon the FDZ and $\Delta CTOD$ as

$$\frac{da}{dN}=\frac{\lambda\pi^2 Y^2(n'+1)}{16C_\varepsilon^2 n'}\left[\frac{C_1E_fV_f}{E_m}\left(1-\frac{dE_f}{2lE_m}\right)+C_2(1-V_f)\right]^2\left(\frac{K'}{R_{p,c}}\right)^3\left(\frac{\Delta\varepsilon_{pl}}{2}\right)^{3n'+1}a \tag{23}$$

The fatigue life formula in the form of the Coffin–Manson law [24,25] is

$$\frac{\Delta\varepsilon_{pl}}{2}=\left\{\frac{32C_\varepsilon^2 n'}{\lambda\pi^2 Y^2(n'+1)}\left[\frac{C_1E_fV_f}{E_m}\left(1-\frac{dE_f}{2lE_m}\right)+C_2(1-V_f)\right]^{-2}\left(\frac{R_{p,c}}{K'}\right)^3\ln\left(\frac{a_f}{a_i}\right)\right\}^{\frac{1}{3n'+1}}(2N_f)^{-1/(3n'+1)} \tag{24}$$

The fatigue life formula in the form of the Basquin law [26] is

$$\frac{\Delta\sigma}{2}=K'\left\{\frac{32C_\varepsilon^2 n'}{\lambda\pi^2 Y^2(n'+1)}\left[\frac{C_1E_fV_f}{E_m}\left(1-\frac{dE_f}{2lE_m}\right)+C_2(1-V_f)\right]^{-2}\left(\frac{R_{p,c}}{K'}\right)^3\ln\left(\frac{a_f}{a_i}\right)\right\}^{\frac{n'}{3n'+1}}(2N_f)^{-n'/(3n'+1)} \tag{25}$$

4. Model application and comparisons

4.1. AA6061-T6

In order to verify our model presented in this study, we first present a quantitative assessment for our basic assumption, i.e. Eq. (5) and determine the value of λ. Under the LSY condition, the CPZ size derived from a modified Dugdale model by Lu and Chow [36] in plane strain condition is

$$r_{cp}=\frac{\pi}{18}\left(\frac{1}{2}+\frac{2}{3}\sqrt{\frac{2}{3}}\frac{\Delta\sigma}{2R_p}\right)\left(\frac{\Delta K}{2R_p}\right)^2 \tag{26}$$

All the parameters have their usual meaning as defined as above. The well-known Dugdale model has been claimed to be valid for both edge-cracked and centre-cracked specimens. Therefore, Eq. (26) can be considered as a valid relationship as well for our case. A numerical comparison between Eqs. (5) and (26) will provide an ideal format for checking the validity and rationality of the present model approach for high-strain LCF. Fig. 4 shows the calculated value of the ratio of the CPZ size to crack length (r_{cp}/a) from Eq. (26) versus the cyclic plastic strain amplitude $\Delta\varepsilon_{pl}/2$ plots for AA6061-T6 at 25 °C. The respective LCF data are taken as in Table 1. Following the example of Mowbray [37], the smooth bar LCF specimen can be represented as a semi-infinite space containing an edge crack, and therefore the value of the crack geometry correction factor Y is 1.12. It is not difficult to show that the predicted r_{cp}/a according to the present model [Eq. (5)] will coincide well with the calculated result from the modified Dugdale model [Eq. (26)] under the general yield condition over a wide range of $\Delta\varepsilon_{pl}/2$ if we take $\lambda=0.19$. From a viewpoint of engineering, this indicates that Eq. (5) can be considered to be sufficiently practical by comparing to the analytical calculation Eq. (26). Therefore, we have so far numerically verified the rationality and validity of the basic assumption of Eq. (5). Naturally, $\lambda=0.19$ is also a reasonable value for the CPZ correction factor of the unreinforced aluminum alloy AA6061 at 25 °C.

In order to predict the LCF life with Eqs. (16) and (17), the initial and critical crack lengths, a_i and a_f are also required. In the present analysis, it is assumed that cracks initiate and grow from a microstructural feature (an initial microscopic-size discontinuity) on the first cycle. The size of the initial microscopic discontinuity in the first cycle can in principle be measured. Several published results in aluminium alloy suggest that initial microscopic discontinuities with a size of around 5 μm are common in high strength aluminium alloys. Therefore, an order of magnitude of $a_i=5$ μm will be adopted here. The critical crack length is estimated as $a_f=2$ mm from the surface measurement of fractured specimens. The comparisons of both Coffin–Manson plot and Basquin plot on experimental and calculated fatigue lives using Eqs. (16) and (17) at 25 °C is shown in Fig. 5. Clearly, the predicted fatigue lives coincide well with the observed fatigue lives over wide ranges of strain/stress amplitudes. Some discrepancies were expected because

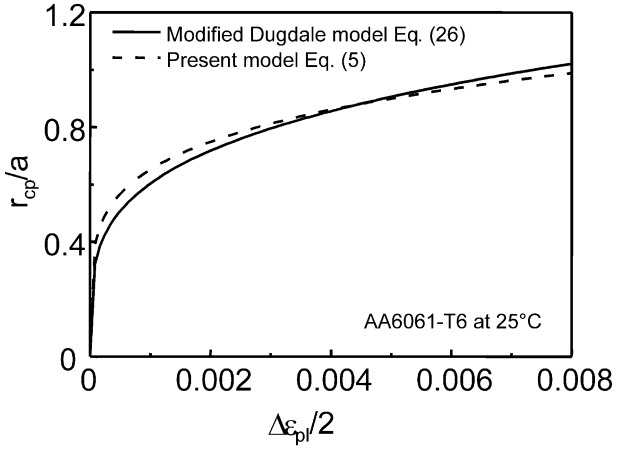

Fig. 4. Comparison of the predicted r_{cp}/a vs. $\Delta\varepsilon_{pl}/2$ plot on AA6061-T6 from the present model [Eq. (5)] and the corresponding result obtained from the modified Dugdale model [Eq. (26)].

the model does not account for strain hardening/softening effects but uses the stress and plastic strain amplitudes that were taken from the hysteresis loops corresponding to half the number of cycles to failure.

4.2. AA6061-20s-T6

In order to calculate the fatigue lives with Eqs. (24) and (25), the values of all other parameters that do not appear in Table 1 are determined as follows. In the same manner of above, it is easy to determine that $\lambda = 0.31$ is a reasonable value for the CPZ correction factor of the short fibre reinforced aluminum alloy 6061 over a wide range of test temperatures. This value of λ is the best value to fit the modified Dugdale model Eq. (26) by Eq. (21). Referring to Friend's work [2], the parameters C_1 and C_2 have been taken as 3/8 and 1, respectively. With these two values of C_1 and C_2, and noticing $R_{p0.2,M} = 368$ MPa, the predicted cyclic yield stress from Eq. (19) gives $R_{p0.2,C} = 1.1R_{p0.2,M} = 405$ MPa, which is in good agreement with the experimental value of 402 MPa in this experiment. As already noted above, $C_\varepsilon = 0.20$ is a reasonable and appropriate average value for the short-fibre constraint in an aluminium alloy matrix, because of the result from Eq. (20) $\Delta\sigma_{eff}/2 = 2.5(\Delta\sigma/2)$ being well consistent with the results of finite element modelling of deformation in short-fibre reinforced MMCs [12]. The initial crack size is approximately taken as $a_i = 5$ μm, and the critical crack size is $a_f = 2$ mm. These two values are consistent with the reported results by Levin and Karlsson [12] on the same composite. Furthermore, experimental observations have shown that in most cases fatigue microcracks initiate during the first cycles close to the surface at rather large fibres, fibres of a larger diameter are more prone to fracture than thinner fibres. The value of 5 μm is to be compared with 3 μm, the measured average diameter of fibres. The value of the crack geometry correction factor Y is again taken as 1.12, in the same manner of Mowbray [37].

Fig. 6 summaries the comparison of Coffin–Manson plots on experimental LCF data of AA6061-20s-T6 and model prediction results using Eq. (24) at −100, 25 and 150 °C, respectively. The comparisons of Basquin plots on experimental and calculated fatigue lives using Eq. (25) from −100 to 150 °C are shown in Fig. 7. These diagrams reveal that the predicted fatigue lives coincide reasonably well with the experimentally observed values over a wide range of strain/stress amplitudes and a wide range of test temperatures. In particular, for the studied composite, the fatigue life is not very sensitive to the tested temperatures. However, Fig. 6 indicates that at 25 °C and at the larger level of $\Delta\varepsilon_{pl}/2$ the predicted fatigue lives are slightly larger than the experimental results. This overestimate in fatigue lives at the larger level of $\Delta\varepsilon_{pl}/2$ is expected because the fatigue damage of the composite AA6061-20s-T6 at 25 °C and at the larger level of $\Delta\varepsilon_{pl}/2$ is dominated by ductility exhaustion

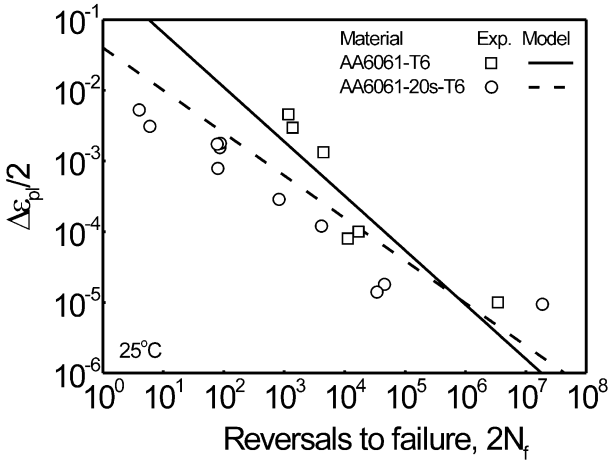

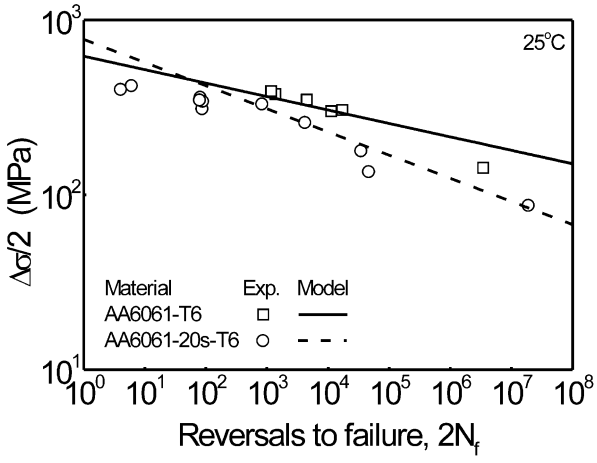

Fig. 5. Comparison of the fatigue lives plots on experimental data and model predictions for AA6061-T6 and AA6061-20s-T6 at 25 °C: (a) Coffin–Manson plots; (b) Basquin plots.

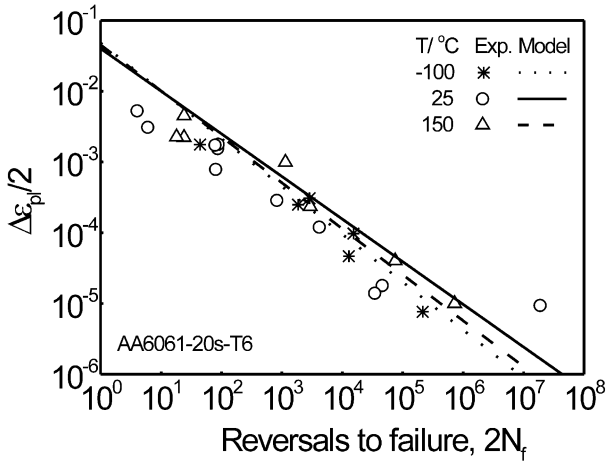

Fig. 6. Comparison of Coffin–Manson plots on experimental data and model predictions for AA6061-20s-T6 at −100, 25 and 150 °C, respectively.

while at the small level of $\Delta\varepsilon_{pl}/2$ by crack propagation. This argument is supported by the specific numerical comparison of the fatigue ductility coefficient ε'_f between the unreinforced AA6061-T6 and the composite AA6061-20s-T6. The predicted ε'_f of AA6061-T6 from Eq. (16) is $\varepsilon'_f = 0.383$, which is nearly 10 times the value of the composite AA6061-20s-T6 predicted from Eq. (24), $\varepsilon'_f = 0.040$. Although the predicted fatigue lives are slightly larger than the experimental results at 25 °C, the predicted fatigue lives are considered to be sufficiently practical from a viewpoint of engineering. The origin of the slight disagreement between the predicted and experimentally observed fatigue lives should be discussed in the near future.

4.3. Comparison of fatigue lives between AA6061-T6 and AA6061–20s-T6

For comparison purpose, the experimental fatigue lives data of AA6061-T6 and AA6061-20s-T6 as well as the corresponding model predictions made using Eqs. (16) and (17) and Eqs. (24) and (25) have also been included in Fig. 5. Clearly, for a given strain/stress amplitude, the experimental fatigue life of the composite AA6061-20s-T6 is shorter than that of the unreinforced AA6061-T6.

Compared with the unreinforced AA6061-T6, the lower LCF life of the composite AA6061-20s-T6 has been reasonably explained in terms of the proposed micromechanical model in this study. The lower LCF life of the composite AA6061-20s-T6 is expected because the addition of high-strength Al_2O_3 fibres in the 6061 aluminium alloy matrix will not only strengthen the microstructure of the 6061 aluminium alloy, but also channel deformation at the tip of a crack into the matrix regions between the fibres and therefore constrain the plastic deformation in the matrix, the overall expected effect is the reduction of the fatigue ductility.

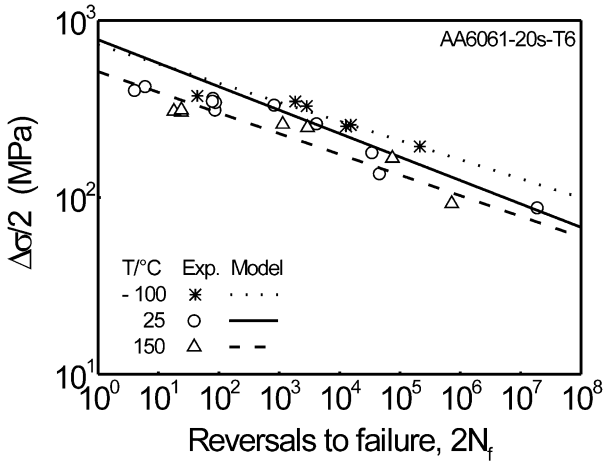

Fig. 7. Comparison of Basquin plots of experimental data and model predictions for AA6061-20s-T6 at −100, 25 and 150 °C, respectively.

5. Discussion

In this article, a LCF model has been developed to predict the fatigue lives of both the unreinforced aluminium alloy and the short-fibre reinforced aluminium alloy MMC based solely on crack propagation from microstructural features. In particular, the near crack-tip cyclic plastic flow and deformation field in randomly-planar oriented short-fibre reinforced MMCs are modeled theoretically for better understanding of the evolution of microstructures by incorporating the constraint exerted by the reinforcement fibres on matrix plasticity and its effect on strain-controlled LCF crack growth processes. In terms of the model, the LCF crack growth rate depends on the range of crack-tip opening displacement. This in turn is a function of the cyclic plastic strain amplitude, the crack length and the constituent parameters. One special advantage of the approach used in the present study is that the physical process of fatigue damage development is clear. It uses only few parameters to establish a connection between the microscopic and macroscopic process of fatigue failure under LCF conditions, all of which can be experimentally determined, based upon microstructural observations.

By comparing Eq. (24) with Eq. (16), we can make the following arguments from the present model prediction. (1) In strain-controlled LCF tests the addition of the reinforcement short fibres in the aluminium alloy 6061 will reduce the fatigue ductility. (2) The MMC with the higher volume fraction of reinforcement short fibres in strain-controlled LCF tests will exhibit shorter fatigue lives than a MMC with a smaller volume fraction. The former has already been shown experimentally in the present study (see Fig. 5), however, the later remains to be verified in the future because of the absence of the data for MMCs with different fibre contents.

It is noteworthy that, although the ΔJ parameter has demonstrated excellent versatility in the correlation of fatigue crack growth for tests with various total-strain or plastic-strain amplitudes [38–42], the methods used in the literature for the calculation of ΔJ are mainly based upon the characteristic values of the deformation behaviour in a stabilised half-life stress–strain hysteresis loop. The method presented in this study, however, provides a new and simplifying method for the calculation of ΔJ under the high-strain LCF conditions. Its special advantage is that it sets up a close correlation between ΔJ and the microstructural processes of the cyclic plastic deformation ahead of the crack tip and therefore provides a more reliable basis for the LCF life prediction of short-fibre reinforced MMCs. In particular, the newly derived ΔJ which incorporates physically measurable quantities is more versatile for complex loading situations.

Comparing Eqs. (16) and Eq. (24) with the standard Coffin–Manson law, $\Delta\varepsilon_{pl}/2 = \varepsilon'_f(2N_f)^c$, the exponent c

in the present study is found to be $-1/(1+3n')$. This result is as same as that reported in the authors' previous model for particulate-reinforced aluminium alloy matrix MMC [16] as well as for short-fibre reinforced pure aluminium matrix MMC [17]. It is noted here that in Tomkin's model [19], $c=-1/(1+2n')$, and in Morrow's model [43], a relationship between c and n' through an energy argument was proposed to be $-1/(1+5n')$. However, to the author's knowledge, so far no general concluding justification can be provided for the relationship between c and n' in particular in particulate and short fibre reinforced MMCs.

It should be interested to assess how sensitive the fatigue life predictions to the values of the initial crack length a_i and the critical crack length a_f are. In terms of our fatigue life model, Eqs. (16), (17), (24) and (25) indicate that $N_f \propto \ln(a_f/a_i)$. Compared with $a_i=5$ μm and $a_f=2$ mm, it is easy to show that N_f will decrease 11.5% for $a_i=10$ μm and decrease 18% for $a_i=15$ μm. Similarly, N_f will decrease 11.5% for $a_f=1$ mm but only increase 3.8% for $a_f=2.5$ mm. Anyway, for reasonable values of a_i and a_f, the predicted fatigue life will change approximately within 20%.

Finally, the fact that the present model describes the fatigue life in the entire range both in terms of the LCF Coffin–Manson law (Figs. 5a and 6) and the HCF Basquin law (Figs. 5b and 7) is remarkable. Traditionally, the Coffin–Manson and the Basquin laws have been regarded as being specifically applicable to LCF and HCF, respectively. The present model is essentially a fatigue crack growth model, i.e. it does not take into account fatigue crack initiation which should occupy a substantial fraction of fatigue life in particular in the range of larger fatigue lives. Therefore, the applicability of the model in the LCF range could be expected, whereas its validity in the HCF range appears somewhat surprising. However, the experimental data are frequently found to satisfy both laws equally well. This is also true for the present data on a short-fibre reinforced aluminium-matrix composite and has, for example, also been found to be valid in the case of particulate-reinforced aluminium alloy MMCs [15]. We simply draw attention to these findings without, however, being able to provide a concluding justification. A possible explanation is that the period of crack initiation is much shorter in MMCs and therefore plays a less dominant role.

6. Conclusions

The present study investigates the LCF behaviour of the unreinforced 6061 aluminium alloy and the short-fibre reinforced 6061 aluminium alloy MMCs. From the results obtained in the present study the following conclusions are drawn:

1. A model has been developed to predict the LCF crack growth behaviour as well as the LCF life of unreinforced 6061 aluminium alloy and short-fibre reinforced aluminium-matrix MMCs.
2. Both the empirical Coffin–Manson and Basquin laws have been derived theoretically that describe well the typical behaviour of both unreinforced 6061 aluminium alloy and short-fibre reinforced aluminium-matrix composites.
3. The strain-controlled LCF behaviour of the unreinforced 6061 aluminium alloy as well as the aluminium alloy AA6061 reinforced with Al_2O_3 fibres with a volume fraction of 20 vol.% has been investigated experimentally for different temperatures in total-strain controlled mode, and comparisons between experimental and predicted fatigue lives have been made. The data presented are in good agreement with predictions from this model, which indicates that the proposed modelling approach is generally applicable to the low-cycle and the high-cycle fatigue life prediction of short-fibre reinforced MMCs.
4. It is remarkable that the addition of high-strength Al_2O_3 fibres in the 6061 aluminium alloy matrix will not only strengthen the microstructure of the 6061 aluminium alloy, but also channel deformation at the tip of a crack into the matrix regions between the fibres and therefore constrain the plastic deformation in the matrix. The overall expected effect is then the reduction of the fatigue ductility.

Acknowledgements

This work was funded by Deutsche Forschungsgemeinschaft (DFG) within the Gerhard-Hess Programme (BI 418/5–2). The authors express their thank to Profesor H. Mughrabi for critical discussions.

References

[1] Clyne TW, Bader MG, Cappleman GR, Hubert PA. The use of a δ-alumina fibre for metal-matrix composites. J Mater Sci 1985;20:85–96.
[2] Friend CM. The effect of matrix properties on reinforcement in short alumina fibre-aluminium metal matrix composites. J Mater Sci 1987;22:3005–10.
[3] Friend CM. The effect of temperature on the tensile strength of short δ-alumina fibre/aluminium alloy metal matrix composites. Scripta Metall 1989;23:33–7.
[4] Clyne TW, Withers P. An introduction to metal matrix composites. Cambridge: Cambridge University Press; 1992.
[5] Towle DJ, Friend CM. Effect of reinforcement architecture on mechanical properties of a short fibre/magnesium RZ5 MMC

manufactured by preform infiltration. Mater Sci Engng A 1994; 188:153–8.
[6] Vedani M, Gariboldi E. Damage and ductility of particulate and short-fibre Al-Al_2O_3 composites. Acta Mater 1996;44:3077–88.
[7] Shang JK, Ritchie RO. Fatigue of discontinuously reinforced metal matrix composites. In: Evertt RK, Arsenault RJ, editors. Metal matrix composites: mechanisms and properties. Boston: Academic Press; 1991. p. 255–85.
[8] Allison JE, Jones JW. Fatigue behavior of discontinuously reinforced metal matrix composites. In: Suresh S, Mortensen A, Needleman A, editors. Fundamentals of metal matrix composites. Boston: Butterworth-Heinemann; 1993. p. 269–94.
[9] Williams DR, Fine ME. Quantitative determination of fatigue microcrack growth in SiC whisker reinforced 2124 Al alloy composites. In: Harrigan Jr WC, Strife J, Dhingra AK, editors. Proc 5th Int Conf on Composite Materials. Warrendale: The Metallurgical Society; 1985. p. 639–45.
[10] Hurd NJ. Fatigue performance of alumina reinforced metal matrix composites. Mater Sci Tech 1988;4:513–7.
[11] Harris SJ. Cast metal matrix composites. Mater Sci Tech 1988;4: 231–9.
[12] Levin M, Karlsson B. Crack initiation and growth during low-cycle fatigue of discontinuously reinforced metal-matrix composites. Inter J Fatigue 1993;15:377–87.
[13] Hartmann O, Kemnitzer M, Biermann H. Influence of reinforcement morphology and matrix strength of metal-matrix composites on the cyclic deformation and fatigue behaviour. Inter J Fatigue 2002;24:215–21.
[14] Kemnitzer M. Diploma thesis, Institut für Werkstoffwissenschaften, Universität Erlangen-Nürnberg, Germany, 2000.
[15] Hartmann O. Doctorate thesis, Institut für Werkstoffwissenschaften, Universität Erlangen-Nürnberg, Germany, 2002.
[16] Ding H-Z, Hartmann O, Biermann H, Mughrabi H. Modelling low-cycle fatigue life of particulate-reinforced metal-matrix composites. Mater Sci Engng A 2002;333:295–305.
[17] Ding H-Z, Biermann H, Hartmann O. Low cycle fatigue crack growth and life prediction of short-fibre reinforced aluminium matrix composites. Inter J Fatigue [in press].
[18] Laird C. The influence of metallurgical structure on the mechanisms of fatigue crack propagation. In Fatigue crack propagation. ASTM STP 415. PA: ASTM; 1967. p. 131–68.
[19] Tomkins B. Fatigue crack propagation-an analysis. Phil Mag 1968;18:1041–66.
[20] Yong JO, Soo WN. Low-cycle fatigue crack advance and life prediction. J Mater Sci 1992;27:2019–25.
[21] Rice JR. Mechanics of crack tip deformation and extension by fatigue. In: Fatigue Crack Propagation. ASTM STP 415. PA: ASTM; 1967. p. 247–309.
[22] Rice JR. A path independent integral and the approximate analysis of strain concentrations by notches and cracks. J Appl Mech 1968;35:379–86.
[23] Eshelby JD. The determination of the elastic field of an ellipsoidal inclusion and a related problem. Proc R Soc A 1957;241:376–96.
[24] Coffin LF. A study of the effects of cyclic thermal stresses on a ductile metal. Trans Amer Soc of Mech Eng 1954;76:931–50.
[25] Manson SS. Behaviour of materials under conditions of thermal stress. National Advisory Commission on Aeronautics: report 1170. Cleveland: Lewis Flight Propulsion Laboratory; 1954.
[26] Basquin OH. The experimental law of endurance tests. Proc of the American Society for Testing and Structures 1910;10:625–30.
[27] Christman T, Needleman A, Suresh S. An experimental and numerical study of deformation in metal-ceramic composites. Acta Metall 1989;37:3029–50.
[28] Shen Y-L, Finot M, Needleman A, Suresh S. Effective plastic response of two-phase composites. Acta Metall Mater 1995;43: 1701–22.
[29] Llorca J, Needleman A, Suresh S. The Bauschinger effect in whisker-reinforced metal-matrix composites. Scripta Metall Mater 1990;24:1203–8.
[30] Davidson DL, McClung RC. Local constraint near fatigue cracks in alloys and particulate composites. Inter J Fract 1997;84:81–98.
[31] Heness GL, Ben-Nissan B, Gan LH, Mai Y-W. Development of a finite element micromodel for metal matrix composites. Comput Mater Sci 1999;13:259–69.
[32] Han NL, Yang J-M, Wang ZG. Role of real matrix strain in low-cycle fatigue life of a SiC particulate reinforced aluminum composite. Scripta Mater 2000;43:801–5.
[33] McCartney LN. Mechanics of matrix cracking in brittle-matrix fibre-reinforced composites. Proc R Soc Lond A 1987;409:329–50.
[34] Covey SJ, Lerch BA, Jayaraman N. Fiber volume fraction effects on fatigue crack growth in SiC/Ti-15-3 composite. Mater Sci Engng A 1995;200:68–77.
[35] Davidson DL. Fatigue crack tip constraint and closure as a function of crack length. In: Ravichandran KS, Ritchie RO, Murakami Y, editors. Small fatigue cracks: mechanics, mechanisms and applications. London: Elsevier Science; 1999. p. 109–18.
[36] Lu TJ, Chow CL. A modified Dugdale model for crack tip plasticity and its related problems. Eng Fract Mech 1990;37:551–68.
[37] Mowbray DF. Derivation of a low-cycle fatigue relationship employing the J-integral approach to crack growth. In: Cracks and fracture. ASTM STP 601. PA: ASTM; 1967. p. 33–46.
[38] Dowling NE. Crack growth during low-cycle fatigue of smooth axial specimens. In: Cyclic stress-strain and plastic deformation aspects of fatigue crack growth. ASTM STP 637. PA: ASTM; 1977. p. 97–121.
[39] Kaisand JR, Mowbray DF. Relationships between low-cycle fatigue and fatigue crack growth rate properties. J Test Eval 1979;7:270–80.
[40] Heitmann HH, Vehoff H, Neumann P. Life prediction for random load fatigue based on the growth behaviour of microcracks. In: Advances in fracture research (Fracture 84), vol. 5. Pergamon Press; 1985. p. 3599–606.
[41] Rie J-T, Wittke H. New approach for estimation of ΔJ and for measurement of crack growth at elevated temperature. Fatigue Fract Engng Mater Struct 1996;19:975–83.
[42] Jung A, Maier H-J, Christ HJ. Low-cycle fatigue behaviour and lifetime prediction of a SiC-particulate reinforced aluminium alloy at elevated temperatures. In: Brown MW, de los Rios ER, Miller KJ, editors. Proc 12th Conf on Fracture, ECF12. Cradley Heath: EMAS; 1998. p. 303–8.
[43] Morrow JD. Cyclic plastic strain energy and fatigue of metals. In: Internal friction, damping and cyclic plasticity. ASTM STP 378. PA: ASTM; 1965. p. 45–84.